

Continuous Surface Cap Model for Geomaterial Modeling: A New LS-DYNA Material Type

Leonard E Schwer

Schwer Engineering & Consulting Services
6122 Aaron Court
WINDSOR CA 95492
707-837-0559
Len@Schwer.net

Yvonne D Murray

APTEK, Inc.
1257 Lake Plaza Drive
COLORADO SPRINGS CO 80906
719-576-8100
Yvonne@APTEK.com

Abbreviations:

ARA Applied Research Associates
CSCM Continuous Surface Cap Model
MPa Mega-Pascal
SRI SRI International
TXC Triaxial Compression Test
TXE Triaxial Extension Test
UCT Unconfined Compression Test

Keywords:

Concrete, Rock, Soil, Cap Model, Damage, Rate Effects, Three Invariant

ABSTRACT

The *Continuous Surface Cap Model* is a new addition to the LS-DYNA geomaterial modeling library of constitutive models (Material Type 145). This new model should replace the use of the Geological Cap Model (Material Type 25) for most applications. The *Continuous Surface Cap Model* maintains all the functionality of the Geological Cap Model with the addition of the third stress invariant, strain rate effects, and damage modeling. The *Continuous Surface Cap Model* has also been reported to be about three times faster than the Geological Cap Model in a large scale application. This article briefly describes some of the model features and illustrates its application.

INTRODUCTION

The unique feature of this model is that the shear failure and compaction (cap) surfaces are ‘blended’ together to form a ‘smooth’ or ‘continuous’ surface. In the work of Schwer and Murray (1994) and Schwer (1994) the descriptions ‘Single Surface’ and ‘Smooth Cap Model’ are used to indicate this feature. Recently, Fossum and Fredrich (2000), who developed a derivative the model, used the term ‘Continuous Surface Cap Model.’ This latter description seems to connote the model’s unique feature and is adopted in this text.

Why another cap model?- The *Continuous Surface Cap Model* evolved from an early DYNA3D implementation by Pelessone (1989), which never became part of the standard DYNA3D distribution, but formulated and implemented the continuous surface approach to cap modeling. This implementation, like the present, included strain sub-incrementing (sub-cycling) which was needed for modeling high energy explosions in soil, e.g. large increments in strain over a small explicit integration time step. Lacking sub-incrementing, the existing DYNA3D, and LS-DYNA, Geologic Cap Model would rapidly deviate significantly from the failure and compaction surfaces and cause the model to produce erroneous results, or halt due to an error condition. This high energy explosion in soil application is also the legacy of the model’s somewhat obscure, and seldom used, Gruneisen ratio Γ and shock parameter S_I representation of the pressure-volume strain response. The Pelessone implementation also included a quadratic representation of the plastic volume strain

$$\varepsilon_V^p = W \left(1 - \exp \left[-D_1 (X(\kappa) - X(\kappa_0)) - D_2 (X(\kappa) - X(\kappa_0))^2 \right] \right)$$

which is more useful in fitting laboratory data than the linear exponent form used in the LS-DYNA Geologic Cap Model.

The model was next adapted to better represent rocks and concrete by introducing the third deviatoric stress invariant J_3' , or equivalently the closely related Lode Angle β , using another unique functional form due to Rubin (1991). The multiplicative form of the third invariant proposed by Rubin was ideally suited to the *Continuous Surface Cap Model* as it already uses a multiplicative form for creating the continuous shear and failure surface from two independent functional forms.

Geological materials experience additional compaction when the compaction is combined with some shear loading. This phenomena is termed *shear enhanced compaction*. Shear enhanced compaction accounts for the difference between the pressure versus volume strain responses measured in hydrostatic and uniaxial strain loading tests. There is also some experimental evidence that the shape of the cap surface (ellipticity) changes as the cap expands. A simple model of shear enhanced compaction is included in the model.

More accurate modeling of the stress-strain response in tri-axial compression testing is possible when the kinematic strain hardening parameters c^α and N are made operative. This is apparently the same shear surface kinematic hardening formulation used in the LS-DYNA Geologic Cap Model, and is attributed to Sandler et al (1984).

For applications involving stress wave propagation in geomaterials, where strain-rate effects are important, a viscoplastic formulation was added by Schwer (1994), and further improved by Murray (1997). The implementation uses a viscoplastic formulation attributed to Duvaut-Lions and popularized in several works of Simo and co-workers; see for example Simo and Hughes (1998). Although a useful addition to the model, the current implementation applies the same rate increase to the shear and failure portions of the model, although experience

indicates that different rates should be used for different stress trajectories, i.e. combinations of shear and compaction.

Most recently, Murray (1995) has added several forms of damage mechanics, based on the formulations of Simo and Ju; see for example Simo et al. (1987). The addition of damage mechanics makes it possible to replicate the strain softening, and eventual failure, of a continuum under compressive loading.

In this paper, the basic model features are described. Sections are included to describe some of the above listed model features and illustrations from various applications are used to demonstrate these model features.

CONTINUOUS SURFACE CAP MODEL

Cap Model Shear Failure Surface

As a basis for comparison, the Geologic Cap Model (Material Type 25) is a traditional two-surface cap model, i.e. the shear failure and compaction surface are defined separately. The *Continuous Surface Cap Model* uses the same form of the shear failure surface as used by the Geologic Cap Model (Material Type 25):

$$\sqrt{J'_2} = F_e(J_1) = \alpha - \gamma \exp(-\beta J_1) + \theta J_1$$

where J_1 and J'_2 are the first and second invariants of the deviatoric stress tensor, respectively, and the Greek symbols are material parameters.

Cap Model Compaction Surface

To form the continuous shear and compaction surface, the functional form of the cap surface introduced by Sandler and Rubin and used by Simo et al. in the Geological Cap Model, is modified:

$$\sqrt{J'_2} = F_c(J_1, \kappa) = 1 - \frac{[J_1 - L(\kappa)][|J_1 - L(\kappa)| + J_1 - L(\kappa)]}{2[X(\kappa) - L(\kappa)]^2}$$

This function form is displayed schematically in Figure 1. The function is unity for $J_1 < L(\kappa)$ and elliptical for $L(\kappa) \leq J_1 \leq X(\kappa)$. As before, κ is a hardening parameter that causes the cap surface to move (expand or contract), $X(\kappa)$ is the position on the J_1 -axis where the outer edge of the ellipse (cap surface) intersects, and $L(\kappa)$ is the position on the J_1 -axis where the ellipse (cap surface) intersects the shear failure surface.

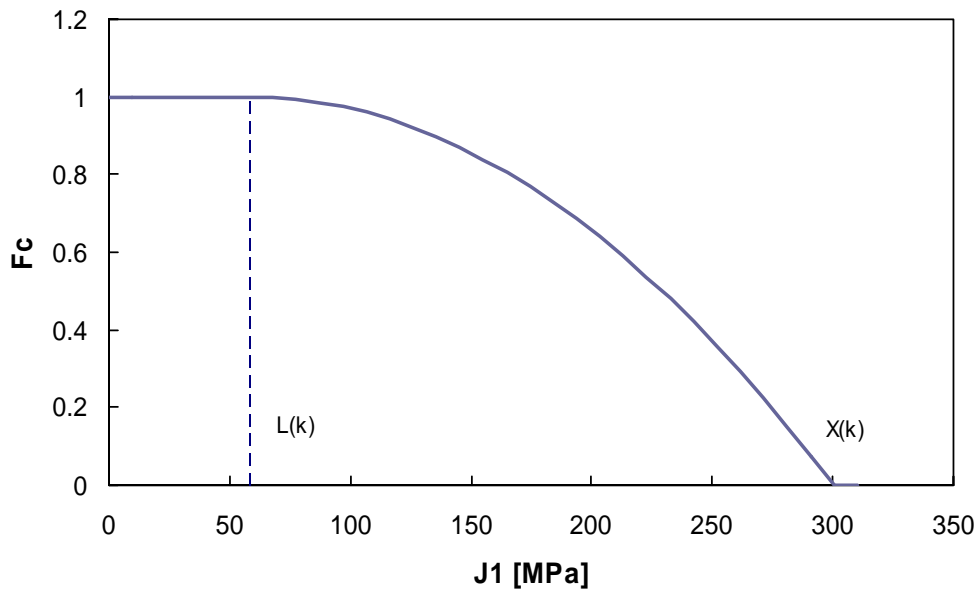


Figure 1 Compaction surface functional form used in Continuous Surface Cap Model.

Continuous Surface

To form the continuous shear and compaction surface, the functional forms of the shear failure and cap surface are multiplied together:

$$\sqrt{J'_2} = F_f (J_1, \kappa) = F_e \sqrt{F_c}$$

The resulting *Continuous Surface Cap Model* is illustrated in Figure 2. For comparison purposes, Figure 3 illustrates the shear and cap surfaces from Material Type 25, for Salem Limestone, and the corresponding surface for the *Continuous Surface Cap Model*. For the purposes of this illustration, no adjustment has been made in the cap shape parameters R even though the *Continuous Surface Cap Model* has a different functional form for the cap surface, and hence typically a different parameter value to best fit the data. Figure 4 shows a sequence of continuous surfaces to illustrate how the *Continuous Surface Cap Model* evolves under increasing loading. Note the shear failure surface, the same as used in Material Type 25, forms an envelope or upper limit for the evolving continuous surfaces.

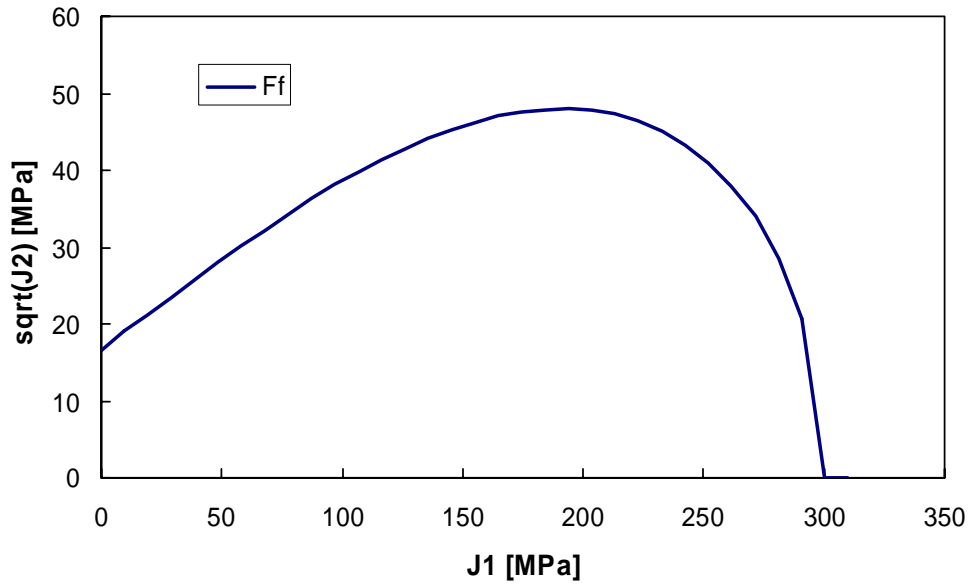


Figure 2 Continuous Surface Cap Model illustration for Salem Limestone.

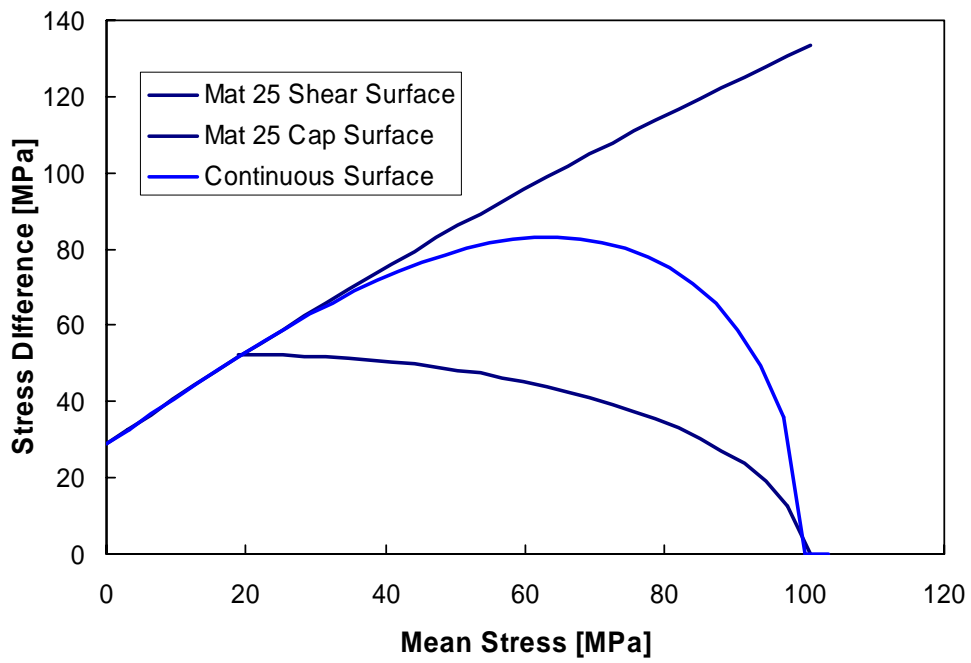


Figure 3 Comparison of two surfaces of Material Type 25 with Continuous Surface Cap Model.

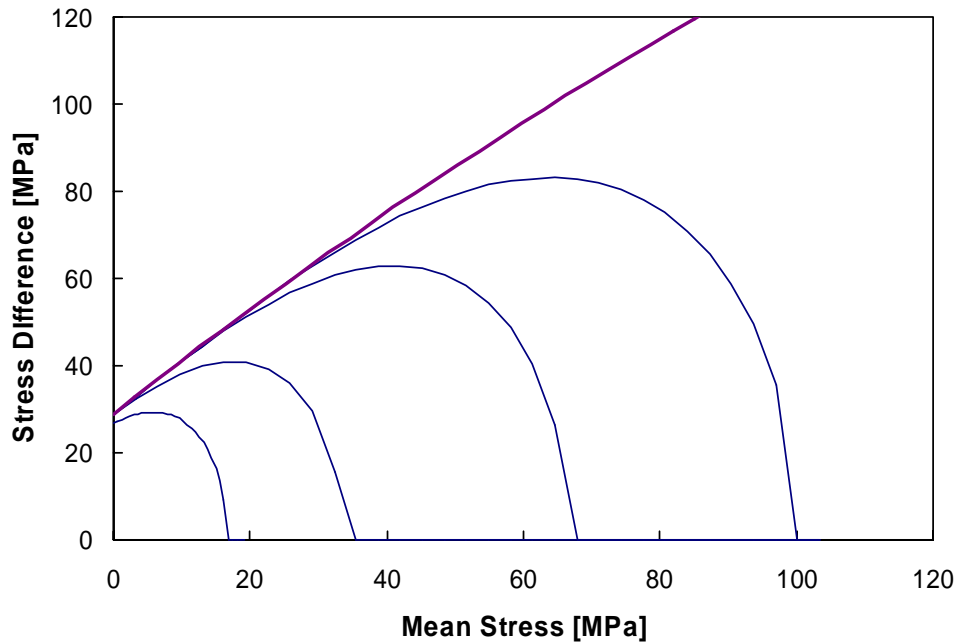


Figure 4 Illustration of evolution of the Continuous Surface Cap Model under increased loading.

THREE INVARIANT FORMULATION

As discussed in the Introduction to Geomaterial Modeling (Schwer, 2001), geomaterials are observed to be weaker in tri-axial extension than tri-axial compression. In tri-axial extension the specimen is loaded hydrostatically and then either:

- The lateral confinement is increased while holding the axial stress constant; called conventional tri-axial compression as the mean stress increases, or
- The lateral stress is held constant, as in tri-axial compression, but then axial load is *decreased*; called reduced tri-axial extension as the mean stress decreases.

Data for Salem Limestone (from ARA) in tri-axial compression (TXC) and tri-axial extension (TXE) is shown in Figure 5. As explained in the Geomaterial Characterization section (Schwer, 2001), and demonstrated here in the Figure 5, the classical Mohr-Coulomb model is a simplest model that *predicts* this observed weaker behavior in tri-axial extension. Figure 6 shows the π -plane view of several classical failure surfaces and graphically indicates the lower failure strength in TXE provided by the Mohr-Coulomb failure criteria.

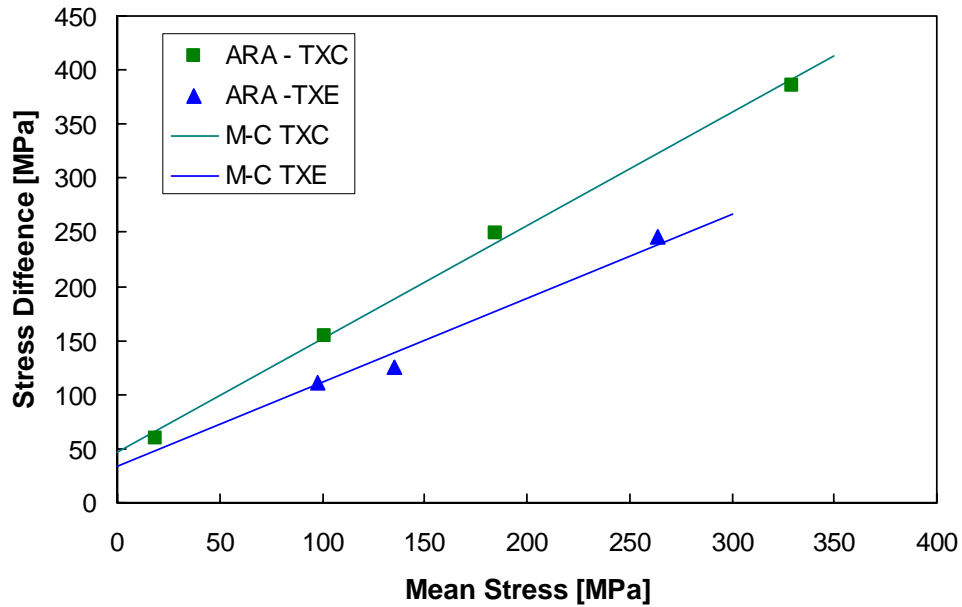


Figure 5 ARA tri-axial compression and extension data for Salem Limestone and the corresponding Mohr-Coulomb fits to the data.

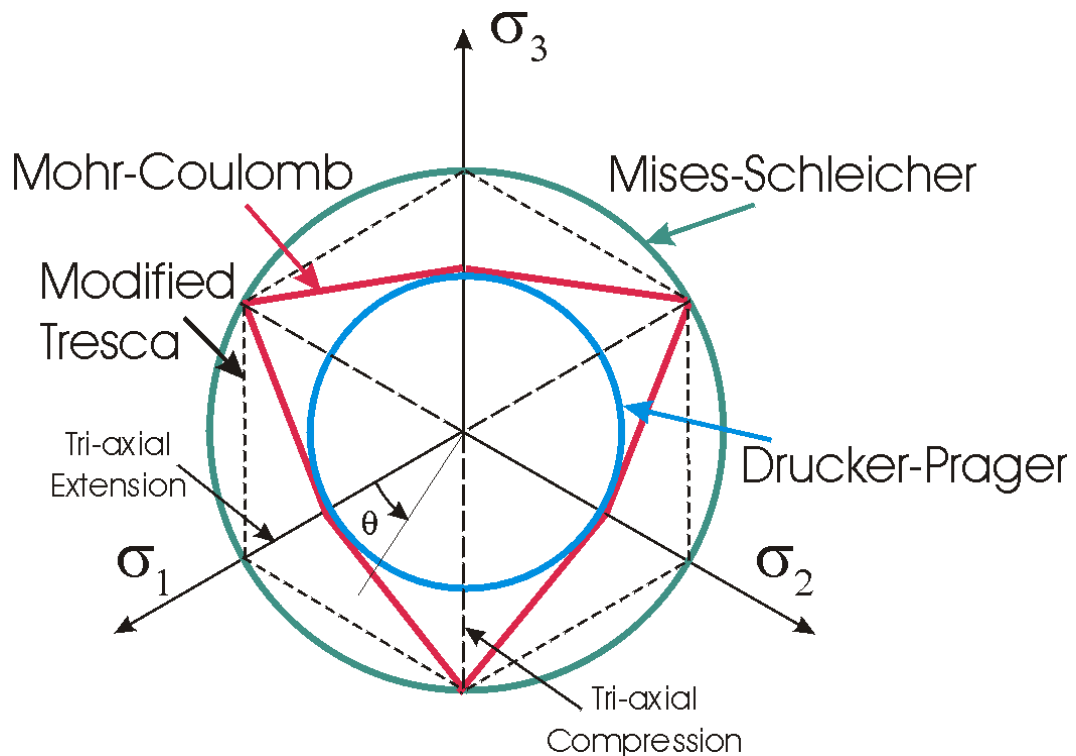


Figure 6 π -plane view of classical yield functions.

The three invariant formulation, Rubin (1991), implemented in the *Continuous Surface Cap Model*, see Figure 7, is very general and can be calibrated to a wide range of tri-axial extension data, beyond the simple linear fit offered by the traditional Mohr-Coulomb model. It also includes as a subset the often referenced Willam and Warnke¹ third

¹ See for example page 352 in Chen and Han (1988).

invariant formulation. However, when such TXE material characterization data is not available, it is recommended that the Mohr-Coulomb form of Rubin's three invariant formulation be used.

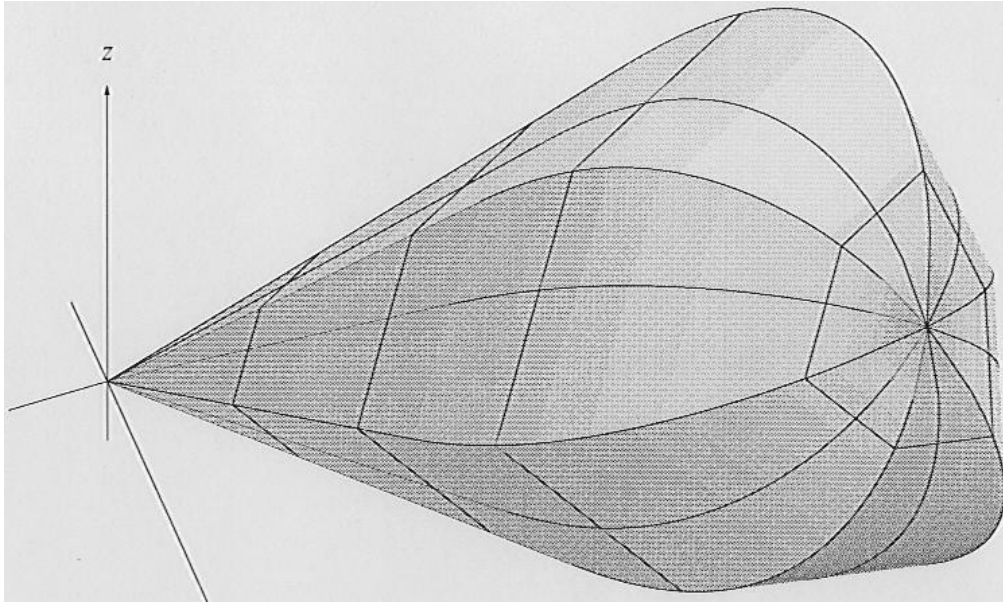


Figure 7 Stress space view of Continuous Surface Cap Model.

Figure 8 compares the ARA measured TXC and TXE data for the case of 50 MPa confinement (TXC) and 50 MPa constant axial stress (TXE) with the *Continuous Surface Cap Model* predictions. Also shown are the classical Mohr-Coulomb TXC and TXE failure surfaces that correspond to the data shown previously in Figure 5. Note the ARA TXE data indicates Salem Limestone is somewhat weaker than predicted by a classical Mohr-Coulomb model.

The same Mohr-Coulomb TXC and TXE simulation exercise was repeated using the Geologic Cap Model (Material Type 25). Figure 9 shows the comparison of the Geologic Cap Model results with the data reported by ARA and the Mohr-Coulomb failure surfaces. As can be seen in this comparison, the TXE response predicted by the Geologic Cap Model exceeds the ARA data and the TXE Mohr-Coulomb failure surface. This demonstrates the two invariant formulation limitations of the Geologic Cap Model. This can be a significant limitation, as in most transient analyses there are likely to be portions of the geological material model that have stress trajectories that are not near the tri-axial compression meridian of the failure surface.

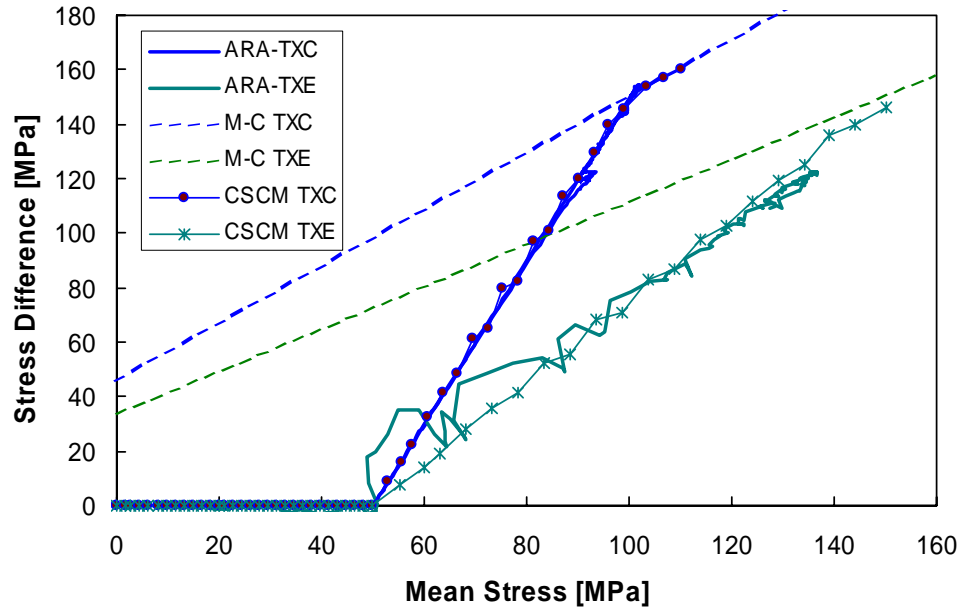


Figure 8 Comparison of ARA Salem Limestone TXC and TXE data and Continuous Surface Cap Model (CSCM) predictions.

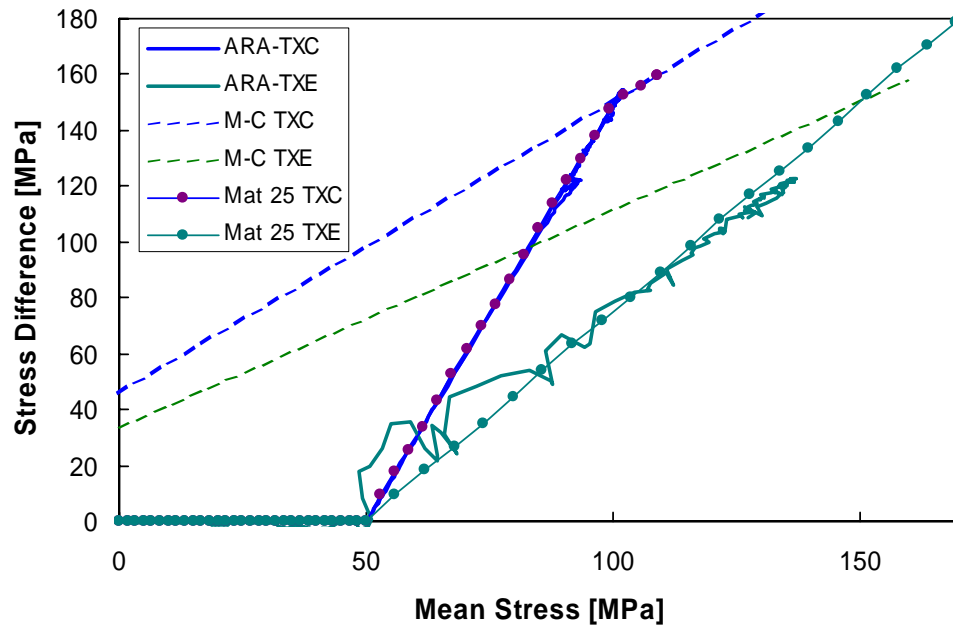


Figure 9 Comparison of ARA Salem Limestone TXC and TXE data and Geologic Cap Model (Material Type 25) predictions.

STRAIN RATE EFFECTS

The viscoplastic formulation implemented in the *Continuous Surface Cap Model* is attributed to Duvaut and Lions (1972) and popularized by Simo et al. (1988). Details of the derivation and a comparison with the more popular Perzyna type model is given in Schwer (1994) and Murray (1997).

The Duvaut and Lions viscoplastic formulation scales the viscoplastic stress update between the elastic trial stress and the inviscid stress update:

$$\sigma_{n+1} = \frac{\sigma_{n+1}^{trial} + (\Delta t / \tau) \bar{\sigma}_{n+1}}{1 + (\Delta t / \tau)}$$

$$\sigma_{n+1}^{trial} = \sigma_n + C : \Delta \epsilon_{n+1}$$

$$\bar{\sigma}_{n+1} = \sigma_n + C : \Delta \epsilon_{n+1}^e$$

using the parameter τ , the relaxation time. Here the trial stress σ_{n+1}^{trial} is simply the elastic stress update and the inviscid stress update $\bar{\sigma}_{n+1}$ is obtained from the solution of the elasto-plastic cap algorithm without rate effects. It is trivial to show that in this viscoplastic update, in the limit, the relaxation time preserves both the elastic and inviscid solutions, i.e.

$$\tau \rightarrow \infty \quad \sigma_{n+1} \rightarrow \sigma_{n+1}^{trial}$$

$$\tau \rightarrow 0 \quad \sigma_{n+1} \rightarrow \bar{\sigma}_{n+1}$$

As a demonstration of the viscoplastic capability of the *Continuous Surface Cap Model*, a comparison is made with the results presented by Katona and Mulert (1984) for a Perzyna type viscoplastic cap model. Katona and Mulert simulated a hypothetical uniaxial strain loading history, as shown in Figure 10, using the cap model parameters for McCormick Ranch Sand².

Figure 11 compares the two stress histories (Perzyna and inviscid) with the *Continuous Surface Cap Model* Duvaut-Lions viscoplastic formulation using a relaxation time of $\tau = 0.25$. Overall the two viscoplastic simulations agree quite well, which is gratifying considering:

1. The two viscoplastic formulations are quite different; although the parameter $\tau = 0.25$ was chosen to match the Perzyna maximum axial stress.
2. The cap models are slightly different; Katona and Mulert used a Sandler and Rubin type cap model.
3. The numerical integration schemes were different; Katona and Mulert used an implicit integration algorithm.

² These cap model parameters were published by Sandler and Rubin (1979) in their original cap model paper.

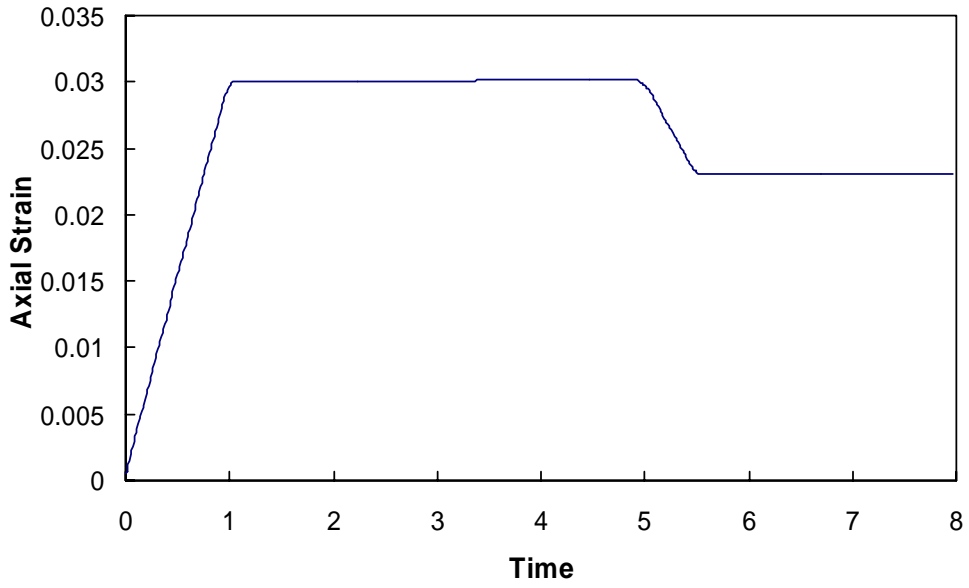


Figure 10 Uniaxial strain loading history.

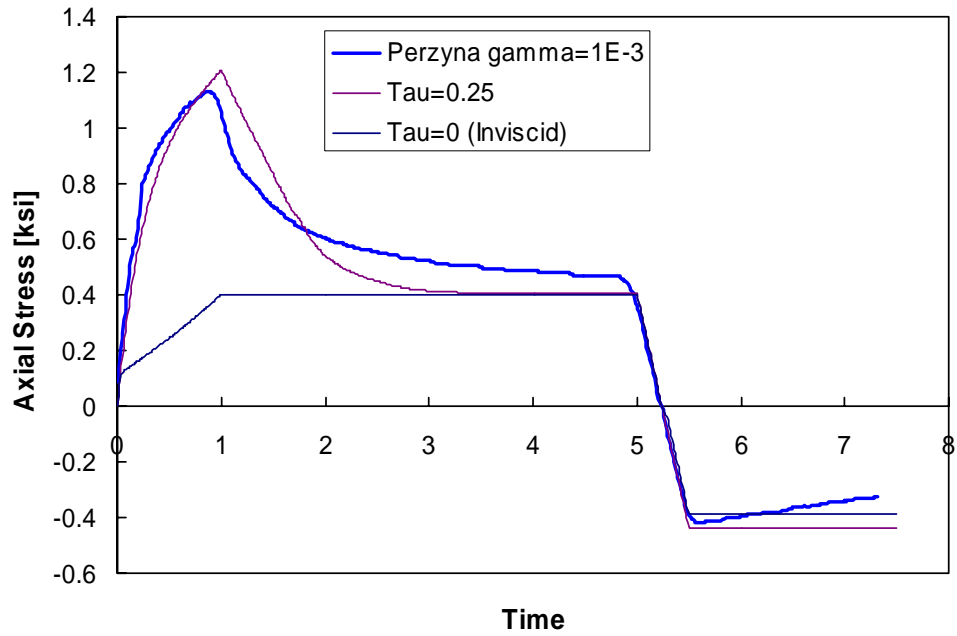


Figure 11 Comparison of Perzyna and Duvaut-Lions viscoplastic axial stress histories.

DAMAGE MODELING

There are two main types of damage included in the *Continuous Surface Cap Model*:

1. Ductile damage that degrades the stress when the mean stress is compressive,
2. Brittle damage that degrades the stress when the mean stress is tensile.

Both types of damage degrade the stress computed from the algorithm without damage, σ_{ij} , to a lesser value based on a scalar damage parameter, i.e.

$$\bar{\sigma}_{ij} = (1-d)\sigma_{ij}$$

where $\bar{\sigma}$ is the damaged stress and d is the damage parameter defined as

$$d = G(\tau) = 1 - \frac{(1-A)r_0}{\tau} - A \exp[B(r_0 - \tau)]$$

where A and B are fitting parameters, r_0 is the threshold for damage, i.e. $d = 0$ if $r_0 < \tau$, and τ is a scalar measure of the strain energy.

This is the basic scalar damage model form proposed by Simo and Ju (1987). It has the basic characteristic that as the strain energy increases, $\tau \rightarrow \infty$, the damage parameter tends to unity $d \rightarrow 1$, and the damaged stress tends to zero $\bar{\sigma} \rightarrow 0$. Figure 12 shows the damage function, $G(\tau)$, with some special cases for the fitting parameters A and B .

The damage models were implemented in the *Continuous Surface Cap Model* by Murray (1994).

Summary

For both ductile and brittle damage, the form of the damage evolution is always the same

$$G(\tau) = 1 - \frac{(1-A)r_0}{\tau} - A \exp[B(r_0 - \tau)]$$

and no damage is accumulated until the strain energy measure τ exceeds the damage threshold r_0 , i.e.

$$d = \begin{cases} 0 & \tau < r_0 \\ G(\tau) & \tau > r_0 \end{cases}$$

Ductile Damage. Compressive mean stress $P > 0$

$$A = A_{ductile} \quad B = B_{ductile} \quad r_0 = r_0^{ductile} \quad \tau_{ductile} = \sqrt{\sigma_{ij}^* \varepsilon_{ij} - P^* \varepsilon_v}$$

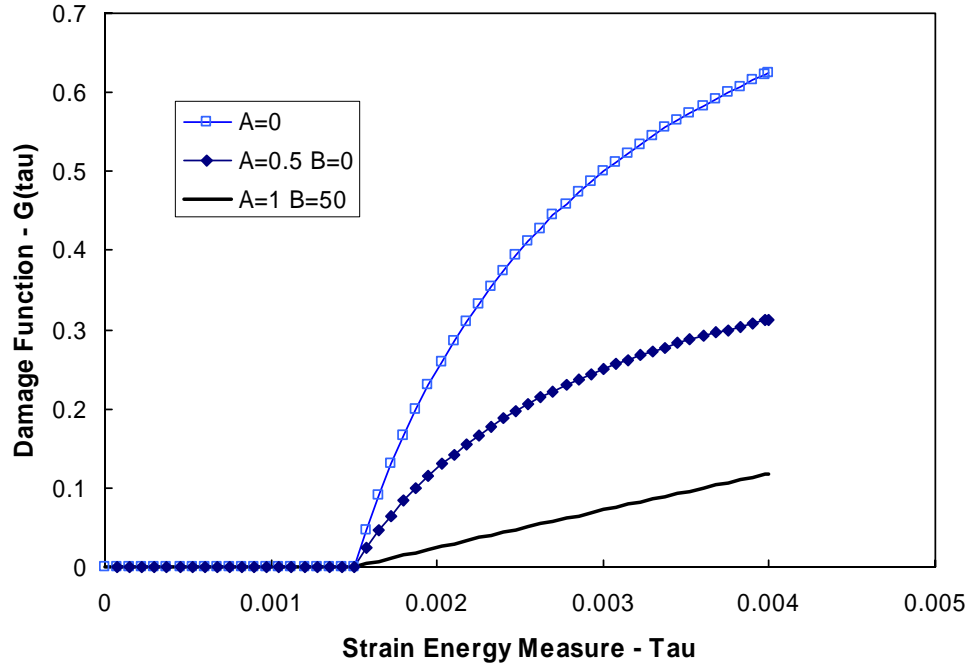


Figure 12 Special cases of the damage function.

Dilation Damage. Compressive mean stress $P > 0$ with tensile volume strain $\epsilon_v < 0$

$$A = A_{dilation} \quad B = B_{dilation} \quad r_0^{dilation} = \frac{\sigma_{max}}{\sqrt{K}} \quad \tau_{dilation} = \sqrt{K \epsilon_v^2}$$

Strain-Based Brittle Damage. Compressive mean stress $P > 0$ with tensile volume strain $\epsilon_v < 0$ (not implemented in the present model)

$$A = A_{brittle} \quad B = B_{brittle} \quad r_0^{brittle} = \frac{\sigma_{max}}{\sqrt{K}} \quad \tau_{brittle} = \sqrt{K \epsilon_v^2}$$

Stress-Based Brittle Damage. Tensile mean stress $P < 0$

$$A = A_{brittle} \quad B = B_{brittle} \quad r_0^{brittle} = \sqrt{\frac{R^2 Y_T^2}{3G} + \frac{P^2}{K}} \quad \tau_{brittle} = \sqrt{\frac{J_2'}{G} + \frac{P^2}{K}}$$

when $Y_T < 0$ then the brittle damage threshold is given by

$$r_0^{brittle} = \frac{\sigma_{max}}{\sqrt{K}}$$

Damage Model Demonstration

Gran and Senseny (1996) report the axial stress versus axial strain response for twelve unconfined compression tests (UCT) on concrete used in scale-model reinforced-concrete wall tests. Two specimen sizes were used for the tests with six tests at each size, i.e. cylindrical specimens with a 2:1 length-to-diameter ratio and diameters of 2 inches

(50.8 mm) and 4 inches (101.6 mm). For each specimen size, the six axial stress-strain responses were fit to parabolic functions of the form:

$$\sigma = E_1 \varepsilon - E_2 \varepsilon^2$$

where σ is the axial stress, ε is the axial strain and E_1 and E_2 are the parameters that best fit the measured data. For the smaller test specimens, the best fit parameters are:

$$E_1 = 29.6 \text{ GPa}$$

$$E_2 = 5.38 \text{ TPa}$$

Figure 13 shows the corresponding unconfined compression test stress-strain response best fit; labeled SRI. The nominal maximum unconfined compressive strength from this fit is 40.7 MPa at a strain of 0.275%. The softening response, shown in Figure 13 is also evident, and was fairly repeatable, in 4 of the 6 tested specimens, out to an axial strain of about 0.45% when Gran and Senseny report loss of stroke control in the testing machine. Also shown in Figure 13 is the model prediction for the UCT without damage.

Using a combination of Ductile and Dilation damage, and some Kinematic Hardening of the initial yield surface, the final comparison between the SRI data and the damage model is shown in Figure 14.

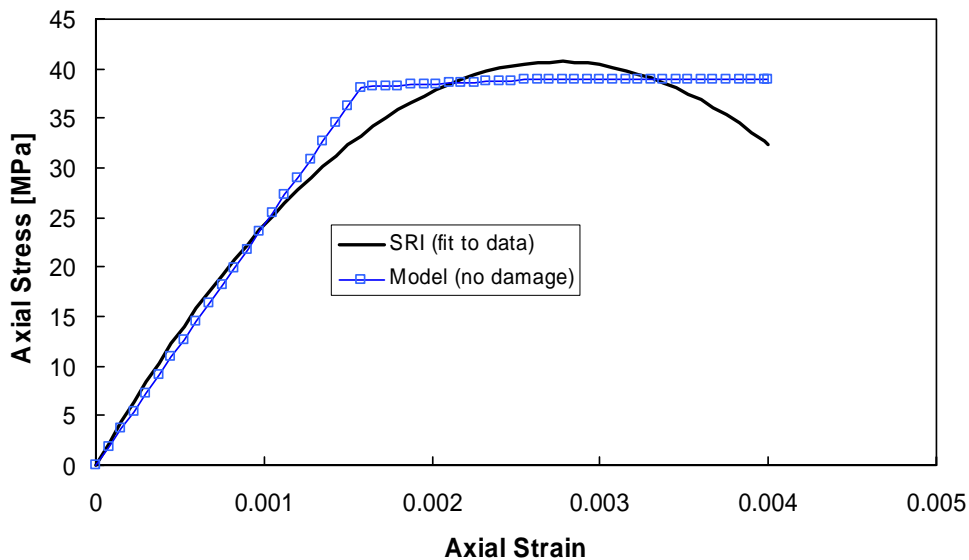


Figure 13 Comparison of SRI unconfined compression test data and model response (without damage).

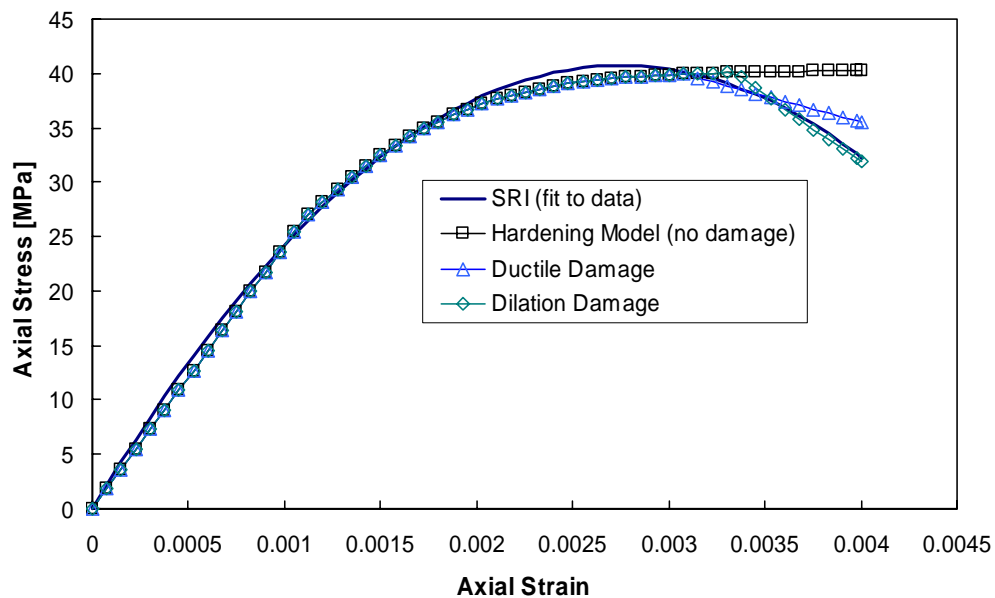


Figure 14 Comparison of SRI data with undamaged, ductile and dilation damaged responses.

CONCLUSIONS

The new *Continuous Surface Cap Model* (Material Type 145) provides several significant improvements over the existing *Geological Cap Model* (Material Type 25):

1. A three invariant formulation which is capable of accounting for observed differences in shear strength under triaxial compression (TXC) and triaxial extension (TXE) conditions.
2. Inclusion of a simple, one parameter, strain-rate effect model which offers users the ability to model viscoplastic response of geomaterials.
3. An extensive damage modeling capability that can be used to simulate details of laboratory tests, or be applied more broadly to predict severe damage in structures.

The above additional features, and others described by Schwer (2001), do come at a cost to the user. More extensive laboratory characterization data is required to calibrate the various additional material model parameters. The user needs to understand which material characterization tests need to be specified and how to interpret the resulting laboratory data for model parameter calibration.

REFERENCES

- Chen, W.F. and Han, D.J. (1988). *Plasticity for Structural Engineers*, Springer-Verlag, New York, NY.
- Fossum, A.F. and Fredrich, J.T. (2000). "Cap Plasticity Models and Compactive and Dilatant Pre-Failure Deformation," Proc. of the Fourth North American Rock Mechanics Symposium, NARMS 2000, Seattle, WA, July 3 – August 1, 2000, pp. 1169-1176.
- Gran, J.K. and Senseny, P.E. (1996). "Compression Bending of Scale-Model Reinforced-Concrete Walls," *ASCE Journal of Engineering Mechanics*, Volume 122, Number 7, pages 660-668, July.
- Katona, M.G. and Mulert, M.A. (1984). "A Viscoplastic Cap Model for Soils and Rocks," C.S. Desai and R.H. Gallagher (Editors), *Mechanics of Engineering Materials*, Wiley, New York, NY, pages 335-350

- Murray, Y.D. (1995). "Numerical Simulation of Damage in Concrete," APTEK, Inc, Technical Report DNA-TR-94-190, prepared for the Defense Nuclear Agency under Contract DNA 001-91-C-0075, November.
- Murray, Y.D. (1997). "Modeling Rate Effects in Rock and Concrete," Proceedings of the 8th International Symposium on Interaction of the Effects of Munitions with Structures, Vol. 1A, April.
- Pelessone, D. (1989). "An Modified Formulation of the Cap Model," Gulf Atomic Report GA-C19579, prepared for the Defense Nuclear Agency under Contract DNA-001086-C-0277, January.
- Rubin, M. (1991). "Simple, Convenient Isotropic Failure Surface," *Journal of the Engineering Mechanics Division*, American Society of Civil Engineers, Volume 117, pages 348-369.
- Sandler, I., DiMaggio, F.L. and Barron, M.L. (1984). "An Extension of the Cap Model: Inclusion of Pore Pressure Effects and Kinematic Hardening to Represent an Anisotropic Wet Clay," in C.S. Desai and R.H. Gallagher, *Mechanics of Engineering Materials*, Chapter 28, Wiley, New York, NY.
- Schwer, L.E. and Murray, Y.D. (1994). "A Three-Invariant Smooth Cap Model with Mixed Hardening," *International Journal for Numerical and Analytical Methods in Geomechanics*, Volume 18, pp. 657-688.
- Schwer, L.E. (1994). "A Viscoplastic Augmentation of the Smooth Cap Model," *Nuclear Engineering and Design*, Vol. 150, pp. 215-223.
- Schwer, L.E. (2001). "Geomaterial Modeling with LS-DYNA," Class Notes for Short Course offered through Livermore Software Technology Corporation., July.
- Simo, J.C., and Ju, J.W. (1987). "Strain and Stress Based Continuum Damage Models – I Formulation," *International Journal of Solids and Structures*, Volume 23, Number 7, pages 821-840.
- Simo, J.C., Kennedy, J.G. and Govindjee, S. (1988). "Non-smooth Multisurface Plasticity and Viscoplasticity . Loading/Unloading Conditions and Numerical Algorithms," *International Journal for Numerical methods in Engineering*, Volume 26, pages 2161-2185.
- Simo, J.C. and Hughes, T.J.R. (1997). *Computational Inelasticity*, Springer-Verlag, New York, NY., ISBN: 0387975209, December.